Effect of sp^2-phase nanostructure on field emission from amorphous carbons

A. Ilie, A. C. Ferrari, T. Yagi, and J. Robertson
Engineering Department, Cambridge University, Cambridge CB2 1PZ, United Kingdom

(Received 26 October 1999; accepted for publication 12 March 2000)

Electron field emission from amorphous carbon is found to depend on the clustering of the sp^2 phase. The size of the sp^2 phase is varied by thermal annealing and it dominates the effect of other parameters, such as chemical composition, surface termination, sp^3 content, or conductivity. The optimum size of the sp^2 phase is determined by Raman spectroscopy and is of the order of 1 nm. The field emission originates from the sp^2 regions and is facilitated by the large field enhancement from more conductive sp^2 clusters in an insulating sp^3 matrix. © *2000 American Institute of Physics.* [S0003-6951(00)04418-1]

Field emission can occur at much lower applied fields from carbon systems than from other materials. The emission can depend on various parameters such as negative electron affinity,[1] band gap,[2] surface termination,[1,3] nitrogen addition,[2,4] depletion layers,[5] and film thickness.[6] In these cases, the emission can be interpreted in terms of homogeneous films and a well-defined band structure.[7] In amorphous carbon, the sp^3 content controls the band gap and electron affinity, while nitrogen addition can shift the Fermi level. However, we recently found by Kelvin probe measurements that sp^3 content and nitrogen addition have a relatively small effect on their work function,[8] which remains in the range 4–5 eV, and so these bulk properties cannot be the fundamental parameters which allow the easy field emission. On the other hand, it is well known that emission occurs at localized sites, rather than uniformly over the surface.[9–11] Carbons with mixed sp^2/sp^3 bonding, like nanocrystalline diamond[12,13] and nanoclustered graphitic films,[11,14] emit at lower fields with a higher emission site density than single-phase films. Scanning tunneling microscopy (STM) also suggests that emission originates from more sp^2 regions.[15,16] This suggests that the sp^2 phase, which has a positive electron affinity, can play an important role in allowing easy field emission. Here, we study the effect of sp^2-phase size on field emission. We find an optimum sp^2 size of $\sim$1 nm.

There are two ways to study the effect of sp^2 size, either varying the deposition conditions or, as here, by postdeposition annealing. Annealing can improve the emission from wide-gap *a*-C:H.[17] Annealing increases the size of sp^2 clusters embedded in the sp^3 matrix until the sp^3 phase completely disappears and the film transforms into nanocrystalline graphite.[18] To distinguish the effects of sp^2 size from other factors such as bonding or surface termination, we studied different amorphous carbons, with and without hydrogen or nitrogen incorporation.

Undoped tetrahedral amorphous carbon (*ta*-C) and lightly nitrogen-doped *ta*-C (*ta*-C:N) with 85% sp^3 bonding were deposited at room temperature by filtered cathodic vacuum arc from 100 eV carbon ions onto n^{++}-Si.[19] A hydrogenated amorphous carbon (*a*-C:H) with an E_{04} gap of 1.7 eV was deposited from methane at room temperature by rf plasma-enhanced chemical-vapor deposition. Hydrogenated tetrahedral amorphous carbon (*ta*-C:H) was deposited from methane using an electron cyclotron wave resonance source at an ion energy of 130 eV.[20] Each set of films is about 50 nm thick, where any thickness dependence of field emission is least.[6]

The films were annealed in a vacuum of 10^{-6} mbar for 20 min to 700 °C for *a*-C:H and to 1000 °C for the other systems. This prevented film oxidation. The film thickness slightly increased at the highest temperatures due to graphitization. Unpolarized Raman spectra were recorded at 514 nm using a Jobin–Yvon T64000 triple-grating spectrometer. The sp^3 content was found by electron energy-loss spectroscopy.[19] The field emission was measured at 10^{-8} mbar pressure in the parallel-plate configuration with a 5-mm-diam cylindrical anode of indium–tin–oxide-coated glass. The interelectrode spacing of 85 μm was defined by adjustable spacers located outside the emission area. This avoided errors due to field enhancement at the edges, or surface leakage on the spacers. To initiate emission, the films were subjected to a series of voltage ramps of increasing maximum voltage. A threshold field F_{th} is defined as the field to give an emission current density of 10^{-6} A/cm^2. Some films such as undoped *a*-C:H are not good emitters, with F_{th} over 20 V/μm, so surface damage is an issue. A slow ramp rate of about 1 V/s and a maximum applied field of 25–35 V/μm were used to minimize surface damage. Our conclusions are based on films that emit at lower fields, where damage is small. Any damage above 25 V/μm decreases F_{th} but does not alter the form of the dependencies seen. The parallel-plate configuration tests only the most emissive spots. Nevertheless, the clear trend in our data is difficult to explain if there was no relationship between field emission and structural changes induced by annealing.

Figure 1(a) shows the effect of annealing temperature on F_{th}. In all systems, F_{th} first decreases, passes through a minimum and then increases again. This common behavior suggests that neither the chemical bonding to H or N, nor surface termination involving C–H bonds are key parameters. Most H evolution from *a*-C:H and *ta*-C:H is above 500 and 600 °C, respectively.[21] Thus, the emission varies mostly at fixed H and N content. The decrease and subsequent in-

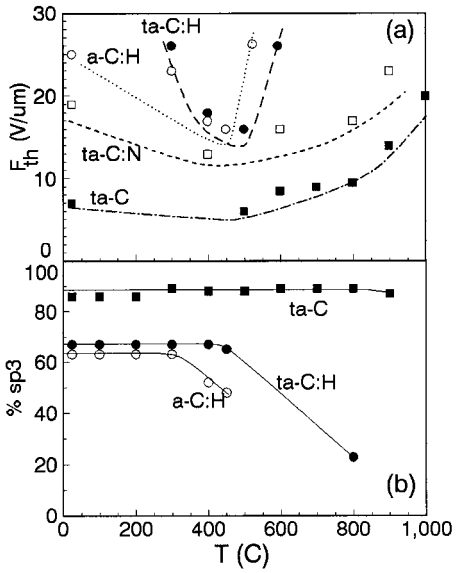

FIG. 1. Variation of (a) the emission threshold field and (b) the film sp^3 content with the postannealing temperature for different amorphous carbon systems.

crease in F_{th} both occur against a continuous increase in conductivity.

Another parameter that can affect the emission is average sp^3 content.[7] Annealing is well known to convert sp^3 sites into sp^2 sites. We now know that the sp^2 phase begins to order before the conversion of sp^3 to sp^2 sites.[22] Thus, Fig. 1(b) shows that the main changes of F_{th} do not generally correspond to changes of sp^3 content for any of the systems studied. Moreover, the decreases of F_{th} occur before the main decrease of sp^3 content, particularly for *ta*-C (where sp^3 content is constant up to 1000 °C) and *ta*-C:H (where sp^3 content first stays constant and then decreases only by 10%). Thus, the sp^3 fraction is not the key parameter.

We now study the role of sp^2 microstructure. Visible Raman spectroscopy is mainly sensitive to sp^2 sites and is a convenient way to follow the evolution of the sp^2 phase. The presence of a Raman *D* peak at $\sim$1350 cm^{-1} indicates that the sp^2 phase is clustering into aromatic rings.[18] There is a relationship[23,24] between the in-plane correlation length L_a of the sp^2 clusters and the intensity ratio of the *D* and *G* peaks, $I(D)/I(G)$. In Fig. 2, from *a*-C to nanocrystalline graphite, $I(D)/I(G)$ increases with increasing L_a (branch 1). For

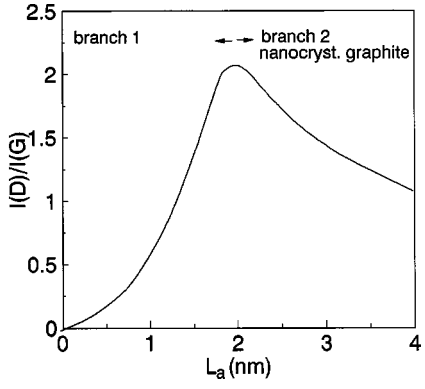

FIG. 2. Generic correlation between the Raman parameter $I(D)/I(G)$ and the in-plane correlation length L_a of the sp^2 aromatic clusters.

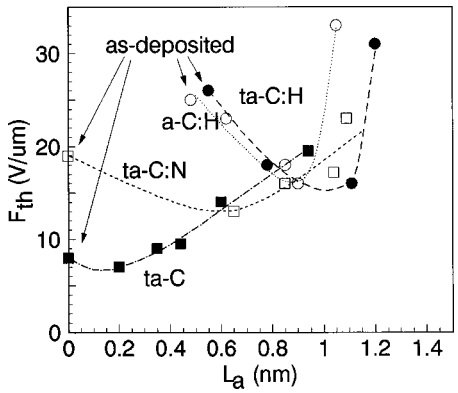

FIG. 3. Dependence of the threshold field F_{th} on the in-plane correlation length L_a of sp^2 aromatic clusters for various amorphous carbon systems.

branch 2 for $L_a > 2$ nm, the transition from nanocrystalline to microcrystalline graphite, $I(D)/I(G)$ decreases as $1/L_a$.[23] Our case is on branch 1. Here, $I(D)/I(G)$ is proportional to the number of rings in a cluster, so $I(D)/I(G)$ increases as L_a^2.[24] $I(D)/I(G)$ is derived from the Raman spectra using a Breit–Wigner–Fano lineshape for the *G* peak and a Lorentzian for the *D* peak.

The dependence of $I(D)/I(G)$ on L_a gives the variation of F_{th} with L_a shown in Fig. 3. There is an optimum size of clusters for each system where F_{th} has a minimum, F_{opt}. Figure 4 plots F_{opt} as a function of L_a. Each system has an optimum cluster size of about 1 nm. In *ta*-C:N, *a*-C:H, and *ta*-C:H the optimum is $L_a \sim 0.7-1.1$ nm and at smaller L_a ~ 0.2 nm in *ta*-C. Figure 3 also shows that F_{th} increases strongly in all the systems when the sp^3 matrix disappears and the material tends towards nanocrystalline graphite. This corresponds to $L_a = 1.5-2$ nm in Fig. 2. This emphasizes the need for both sp^2 and sp^3 phases for good emission.

Nanostructured carbon, nanocrystalline diamond, and carbon nanotubes are the types of carbon that emit at lowest applied field. In microcrystalline diamond, emission is found to occur from grain boundaries,[9,25,26] that is, nm-scale sp^2-bonded regions of positive electron affinity. Similarly, emission from carbon nanotubes[27] occurs from 1 nm curved regions. Our experiments above indicate that nm-scale inhomogeneities also promote emission from *a*-C.

Why is this small length scale so prevalent in such diverse systems? Electron energy distribution (EED) measurements show that electrons are emitted from near the Fermi

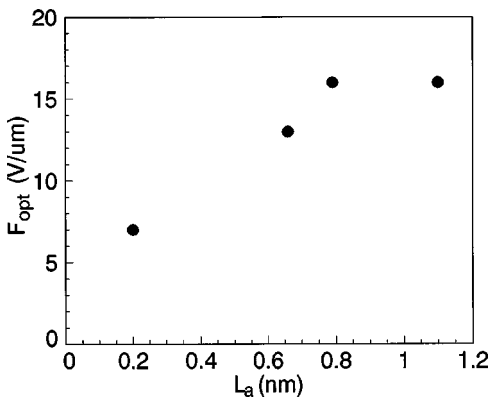

FIG. 4. Variation of the optimum threshold field F_{opt} with L_a.

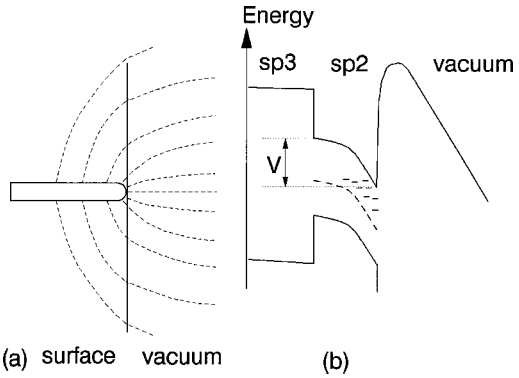

FIG. 5. (a) Field focusing around a high-aspect ratio filament nanostructure. (b) Band model for field emission from filament-type sp^2 clusters perpendicular to the film/vacuum interface.

level, so the potential barrier for emission is the work function, 4–5 eV.[27,28] Second, the EED width shows that emission occurs in the presence of large local fields of thousands of V/μm. So far, the EED shows no evidence of hot-electron effects or conduction-band emission in these systems.

There are numerous mechanisms which can lower the barrier by 0.5–2 eV, such as surface depletion, changes in the surface termination, etc.[7] However, the only effective means to lower the barrier by 4–5 eV is field enhancement. Field enhancement can occur at interfaces between sp^3 and sp^2 phases or at a triple junction between the sp^2 and sp^3 phases and vacuum because of high-aspect ratio geometries and/or the presence of space-charge distributions. Conductive filaments normal to the film surface, such as grain boundaries in microcrystalline diamond, can cause large local electric fields. Conductive filaments and surface regions were observed on *ta*-C surfaces.[28,29] The field lines will focus onto such filaments or grain boundaries, Fig. 5(a). The positive potential on the anode creates negative space charge in the film. sp^2-bonded filaments possess amphoteric gap states around the Fermi level, which become negatively charged [Fig. 5(b)]. The filaments are distributed inhomogeneously in the film so the field lines focus onto the filaments, creating a field enhancement. The local field is enhanced by β compared to the macroscopic field of 1–10 V/μm. β can be over 100 for a filament at the interface with vacuum, giving local fields of thousands of V/μm. For *a*-C:H and *ta*-C:N, from the Fowler–Nordheim plots for the optimum films, we obtain $\beta \sim 490$ and 640, respectively. For this we used barriers for emission ϕ_b of 4 eV for *a*-C:H and 4.5 eV for *ta*-C:N.[8] If the density of states is $N \sim 10^{21}\,\mathrm{cm}^{-3}$ and the charged length of filament is 1.5 nm, the barrier ϕ_b is fully lowered at macroscopic fields of $\sim$10 V/μm. This size is similar to that found here by Raman.

We believe field emission occurs from localized conducting regions because this simultaneously gives large field enhancement and the sizable local conductivity able to support emission. The critical diameter of a filament is a trade off between the need for field enhancement and the need to carry emission current. The macroscopic emission current density J is given in terms of filament diameter d, its conductivity σ_{loc}, emission site density N, and local field F_{loc} as $J = N(\pi d^2/4)\sigma_{\mathrm{loc}} F_{\mathrm{loc}}$. Using $J = 5\times10^{-3}\,\mathrm{A/m^2}$ $N \sim 10^6\,\mathrm{sites/m^2}$, and $\sigma_{\mathrm{loc}} \sim 1\,\Omega^{-1}\,\mathrm{m}^{-1}$ for a typical disordered sp^2 material, we obtain $d \sim 0.7\,\mathrm{nm}$ for $F_{\mathrm{loc}} = 5\times10^9$ V/m.

Even in good emitters, nondestructive conditioning occurs. We attribute this to a combination of current-induced conversion of sp^3 to sp^2 sites, as found by STM,[15,16] and loss of surface hydrogen. Both processes form preferential emitting regions.

In conclusion, we show that the size of the sp^2 phase can dominate the effect of chemical bonding, sp^3 content, or conductivity on field emission. Nanometer-scale sp^2 clusters embedded in the sp^3 matrix were observed using Raman spectroscopy. These can enhance the local field and significantly lower the surface tunnel barrier, explaining the easy emission from mixed-phase carbon systems.

The authors thank V. Stolojan for EELS measurements, A. Hart and S. Rodil for sample preparation, and C. E. Bottani for Raman facilities. A.C.F. thanks the EU for a Marie-Curie scholarship.

[1] M. W. Geis, J. C. Twichell, J. Macaulay, and K. Okano, Appl. Phys. Lett. **67**, 1328 (1995).
[2] B. S. Satyanarayana, A. Hart, W. I. Milne, and J. Robertson, Appl. Phys. Lett. **71**, 1430 (1997).
[3] A. Hart, B. S. Satyanarayana, J. Robertson, and W. I. Milne, Appl. Phys. Lett. **74**, 1594 (1999).
[4] G. A. J. Amaratunga and S. R. P. Silva, Appl. Phys. Lett. **68**, 2529 (1996).
[5] M. W. Geis, J. C. Twichell, and T. M. Lyszczarz, J. Vac. Sci. Technol. B **14**, 2060 (1996).
[6] R. D. Forrest, A. P. Burden, S. R. P. Silva, L. K. Cheah, and X. Shi, Appl. Phys. Lett. **73**, 3784 (1998).
[7] J. Robertson, Mater. Res. Soc. Symp. Proc. **417**, 217 (1997); J. Vac. Sci. Technol. B **17**, 659 (1999).
[8] A. Ilie (unpublished).
[9] N. S. Xu, Y. Tzeng, and R. V. Latham, J. Phys. D **26**, 1776 (1993).
[10] A. A. Talin, L. S. Pan, K. F. McCarty, H. J. Doerr, and R. F. Bunshah, Appl. Phys. Lett. **69**, 3842 (1996).
[11] B. F. Coll, J. E. Jaskie, J. L. Markham, E. P. Menu, A. A. Talin, and P. von Allmen, Mater. Res. Soc. Symp. Proc. **498**, 185 (1998).
[12] W. Zhu, G. P. Kochanski, and S. Jin, Science **282**, 1471 (1998).
[13] M. Q. Ding, D. M. Gruen, A. R. Krauss, O. Auciello, T. D. Corrigan, and R. P. H. Chang, J. Vac. Sci. Technol. B **17**, 705 (1999).
[14] G. A. J. Amaratunga, New Diamond Frontier Carbon Technol. **9**, 31 (1999).
[15] T. W. Mercer, N. J. DiNardo, J. B. Rothman, M. P. Siegal, T. A. Friedmann, and L. J. Martinez-Miranda, Appl. Phys. Lett. **72**, 2244 (1998).
[16] C. Arena, Ph.D. thesis, Cambridge University (1999).
[17] A. P. Burden, R. D. Forrest, and S. R. P. Silva, Thin Solid Films **337**, 257 (1999).
[18] J. Robertson, Prog. Solid State Chem. **21**, 199 (1991).
[19] P. J. Fallon, V. S. Veerasamy, C. A. Davis, J. Robertson, G. A. J. Amaratunga, W. I. Milne, and J. Koskinen, Phys. Rev. B **48**, 4777 (1993).
[20] N. A. Morrison, S. Muhl, S. E. Rodil, A. C. Ferrari, M. Nesladek, W. I. Milne, and J. Robertson, Phys. Status Solidi A **172**, 79 (1999).
[21] J. Ristein, R. T. Stief, L. Ley, and W. Beyer, J. Appl. Phys. **84**, 3836 (1998).
[22] A. C. Ferrari, B. Kleinsorge, N. A. Morrison, A. Hart, V. Stolojan, and J. Robertson, J. Appl. Phys. **85**, 7191 (1999).
[23] F. Tuinstra and J. L. Koening, J. Chem. Phys. **58**, 1126 (1970).
[24] A. C. Ferrari and J. Robertson, Phys. Rev. B (to be published).
[25] C. Wang, A. Garcia, D. Ingram, M. Lake, and M. E. Kordesch, Electron. Lett. **27**, 1459 (1991).
[26] A. V. Karabutov, V. D. Frolov, S. M. Pimenov, and V. I. Konov, Diamond Relat. Mater. **8**, 763 (1999).
[27] O. M. Küttel, O. Gröning, C. Emmenegger, L. Nilsson, E. Maillard, L. Diederich, and L. Schlapbach, Carbon **37**, 745 (1999).
[28] O. Gröning, O. M. Küttel, P. Gröning, and L. Schlapbach, Appl. Phys. Lett. **71**, 2253 (1997); J. Vac. Sci. Technol. B **17**, 1064 (1999).
[29] N. Missert, T. A. Friedmann, J. P. Sullivan, and R. G. Copeland, Appl. Phys. Lett. **70**, 1995 (1997).